ACS Sustainable Chemistry & Engineering

pubs.acs.org/journal/ascecg

Research Article

Glycerol and Maleic Anhydride-Based Acrylic Polyester: A Solution for Greener Photocurable Resins for 3D Printing of Renewable Materials

Gabriel I. dos Santos, Caroline Gaglieri, Rafael T. Alarcon, Aniele de Moura, Fernanda B. dos Santos, and Gilbert Bannach*

Cite This: ACS Sustainable Chem. Eng. 2025, 13, 9771−9782

Read Online

ACCESS | Metrics & More | Article Recommendations | Supporting Information

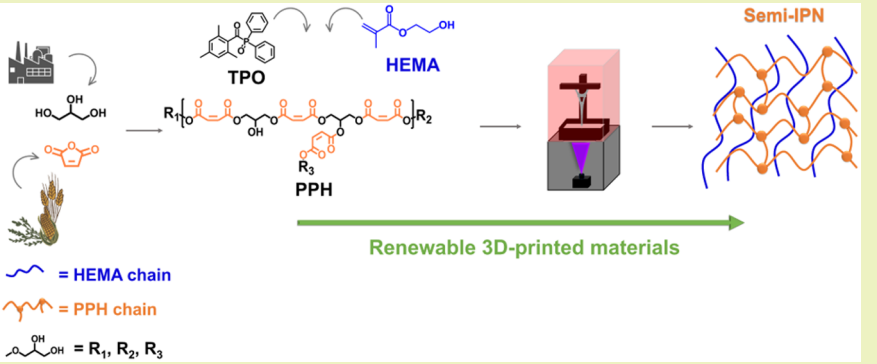

ABSTRACT: The three-dimensional (3D) printing field has emerged as a powerful tool for manufacturing complex design materials, becoming a solution for technological issues, and the depletion of nonrenewable sources brings the urgency of a sustainable additive manufacturing way to produce materials. In this sense, a potentially 100% renewable glycerol and maleic anhydride-based acrylic polyester (PPH) was synthesized, requiring 8 min of reaction after optimization. Then, varied levels of potentially biobased resins were formulated by mixing the renewable polyester, 2-hydroxyethyl methacrylate (as a reactive diluent), and the photoinitiator diphenyl(2,4,6-trimethylbenzoyl)phosphine oxide. These formulated resins were then applied in a digital light processing 3D printer. The resins with PPH content above 50.0% presented suitable viscosity for 3D printing, while the formulation with a lower viscosity value favors printability and resolution for complex design objects. The 3D-printed objects were characterized regarding thermal and mechanical properties, which were verified to be affected by monomer conversion and the amount of PPH in the formulation. High and intermediate amounts of renewable polyester resulted in flexible materials, whereas reducing PPH content produced rigid materials with a substantial increase in hardness. Finally, it is suggested that the difference in reactivity of PPH and HEMA led to the formation of a semi-interpenetrating polymer network. This sustainable approach enabled the production of potentially greener photocurable resins for additive manufacturing.

KEYWORDS: *renewable polymers, sustainable additive manufacturing, digital light processing 3D printing, greener monomers, radical photopolymerization*

1. INTRODUCTION

Since the beginning of time, humans have sought to develop materials with superior qualities to those that nature offers. Thus, polymers have stood out as promising materials since their emergence due to their properties and versatility. However, most of these materials are derived from nonrenewable sources and have a low decomposition rate, contributing to the emergence of white pollution, which negatively impacts the environment.[1,2] Thus, using renewable raw materials to produce polymers promotes sustainability and contributes to a more sustainable and resilient economy.[3] Therefore, renewable inputs such as vegetable oils, terpenes, and glycerol have been researched in the literature to produce renewable polymers.[4−6]

Consequently, given the growing global environmental awareness, there is an increasing trend toward developing green technologies. Thus, the chemical industry has been developing new materials and production processes that minimize environmental impacts, such as biodiesel.[7] However,

Received: April 2, 2025
Revised: June 4, 2025
Accepted: June 5, 2025
Published: June 12, 2025

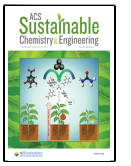

https://doi.org/10.1021/acssuschemeng.5c03006
ACS Sustainable Chem. Eng. 2025, 13, 9771−9782

large-scale production of this biofuel generates a significant surplus of glycerol, a byproduct of the transesterification reaction of oils or fats.[8]

Although often regarded as industrial waste, glycerol is far from being merely a disposal burden.[9] In terms of abundance, low cost, and renewable origin, this compound is highly sustainable, making it a valuable feedstock with economic and environmental benefits for the manufacturing sector. Structurally, the presence of three hydroxyl groups facilitates extensive functionalization, positioning it as a strategic input for several industries, particularly in the production of renewable polymers and other biobased materials. Glycerol is a potential renewable compound that can be used in polymer production without modification or subjected to simple reactions such as esterification, enabling structural changes for its use as a biobased component in materials. Due to these characteristics, glycerol was selected for this work to contribute to the structure of a green polyester intended for potentially biobased photocurable resins.

Furthermore, concerns about sustainable polymer production have driven the demand for inputs that allow the production of materials with properties similar to or better than those observed in materials from nonrenewable sources. In this sense, maleic anhydride emerges as a polyfunctional platform molecule that can be widely used to produce alkyd resins, polymers, and intermediates in the fine chemical industry.[10] Maleic anhydride is traditionally produced by the oxidation of petrochemical compounds such as butane and benzene.[11] However, a more sustainable method for producing this valuable compound for polymer applications involves the use of 1-butanol and furfural—the latter being derived from agricultural waste and biomass, such as corncobs, sawdust, and oat hulls.[10−12] The use of maleic anhydride not only contributes to desirable polymer properties but also supports more sustainable production methods by minimizing the generation of toxic byproducts and reducing the carbon footprint. Moreover, the two carbonyl groups in maleic anhydride enable nucleophilic acyl substitution reactions with alcohols and amines; it can also react with epoxides, by a bimolecular nucleophilic substitution (S_N2) reaction, usually used in ring-opening polymerization (ROP) to provide polyesters.[13−15] Therefore, in addition to its high reactivity, maleic anhydride was selected for this work due to its strong potential for biobased production, thereby increasing the renewable content of the resulting polymers.

The polycondensation reaction between glycerol and cyclic anhydrides has been explored for producing renewable polyesters. As demonstrated by Kolbuk et al. and coauthors,[13] glycerol can react with succinic anhydride to obtain an oligomer, Poly(Glycerol Succinate). This compound was used as an additive for synthetic poly(L-lactic acid) and poly(L-lactide-*co*-caprolactone), aiming for medical applications due to its nontoxic and plasticizer characteristics. As reported by Huang et al.[16] a hyperbranched polyester (HBPE) was synthesized by reacting glycerol and maleic anhydride using a solvent-free method for 4 h without a catalyst. This approach allowed the production of a suitable material for use as a wood adhesive. They also verified that the viscosity of the final product is intrinsically related to the time of reaction and the increase of the oligomer chain, in which long times of reaction lead to high viscosity values. Besides, glycerol and maleic anhydride can be used as a nonbiocidal wood preservation system[17] or as an environmentally friendly polyester for improving the anti-swelling efficiency of wood structures.[18] Although the esterification reaction is explored for obtaining polyester from glycerol and unsaturated cyclic anhydrides, until the moment, there are no reports in the literature for the use of these α,β-unsaturated (or α,α-unsaturated) polyesters produced from these renewable precursors in the production of photocurable polymers. The high reactivity of alkenes within the polyester structure suggests a promising avenue for radical polymerization, potentially leading to polymers with high biobased content, faster reaction times, and new properties.

The oligomers (also called prepolymers) with these characteristics can be applied as renewable acrylic monomers for photopolymerization and in photo three-dimensional (3D) printing.[19] However, these monomers used to have high viscosity due to the high degree of cross-linking between their long and branched polyester chains and the strong molecular interactions, such as hydrogen bonding, making their application in 3D printers difficult. To overcome this issue, 2-hydroxyethyl methacrylate (HEMA) can be used as a low molecular weight and low viscosity reactive diluent.[20,21] HEMA was selected for this work since it can be considered biobased when this methacrylic ester of ethylene glycol is produced indirectly by fermentation of xylose from *Escherichia coli* (for production of ethylene glycol) and by catalytic oxidative dehydrogenation of biosynthetic isobutyric acid (for production of methacrylic acid).[22,23] The physical characteristics of HEMA (mainly its viscosity and low stability for photopolymerization) limit its isolated use in the photo 3D printing process, thus requiring its combination with other acrylic compounds. Ng et al.[24] obtained a photocurable polymer for 3D printing from mixtures of PEGDA (which has a controllable viscosity) and HEMA. At the same time, Cui et al.[25] produced dynamic thermosetting photopolymers from 2-hydroxyethyl Acrylate (HEA) and HEMA systems that were applied in 3D printing. Finally, beyond the potentially biobased character, the mixture of HEMA with other monomers complements its properties, providing a mixture with ideal viscosity for use in 3D printers and accessing high reactivity.

In our strategy, a prepolymer from glycerol and maleic anhydride was prepared for the first time in 8 min by one-pot and solvent-free reaction. This approach allows the preparation of α,β-unsaturated dicarboxylic polyesters that can be used for radical photopolymerization and then applied in the formulation of biobased acrylic resins as the viscous counterpart of the low viscosity of HEMA, which was used as a reactive diluent in the mixture. Although other studies have also synthesized and used this polyester, to the best of our knowledge, this is the first time that the polyester from glycerol and maleic anhydride has been applied in the formulation of potentially biobased resins for additive manufacturing.

2. EXPERIMENTAL SECTION

2.1. Materials. Glycerol (GLY) was purchased from Merck. Maleic anhydride (MA), sulfuric acid (H_2SO_4; 95%), diphenyl(2,4,6-trimethylbenzoyl)phosphine oxide (TPO; 97%), and 2-hydroxyethyl methacrylate (HEMA; 99%) were purchased from Sigma-Aldrich and used as received. The commercial resin RP-405 (CR) was acquired from 3DFila.[26]

2.2. Prepolymer Syntheses from Glycerol and Maleic Anhydride. Two solvent-free and one-pot syntheses were performed to produce a prepolymer. The first synthesis, following a literature procedure,[27] involved reacting glycerol and maleic anhydride in a 2:3 molar ratio (GLY/MA) under the mildest possible conditions. GLY (19.3 g) was added to a beaker covered with aluminum foil and heated to 80 °C for 15 min before the addition of maleic anhydride (30.8 g).

https://doi.org/10.1021/acssuschemeng.5c03006
ACS Sustainable Chem. Eng. 2025, 13, 9771−9782

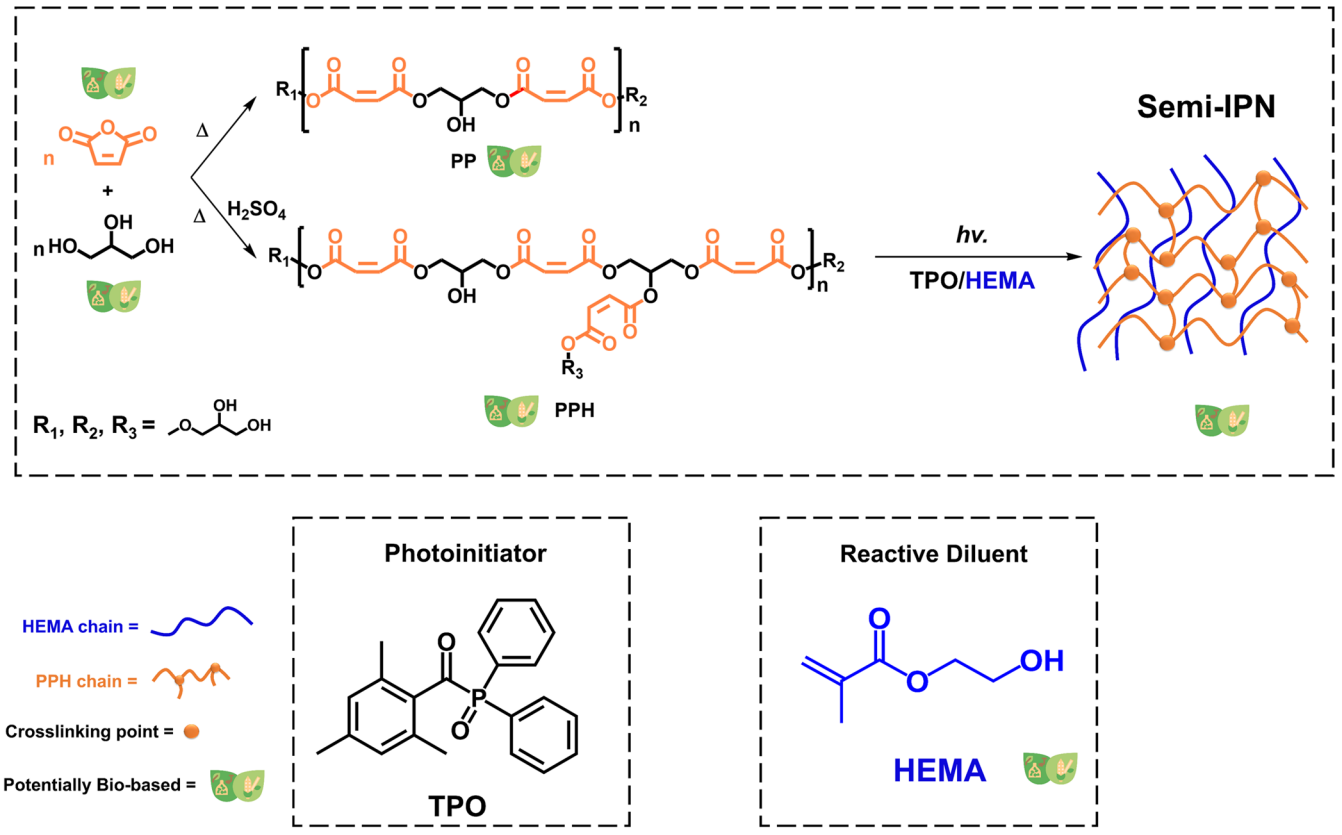

Figure 1. Scheme of the preparation steps for prepolymers using a catalyst (or not), the photopolymerization reaction of the formulated resins, the Type I photoinitiator, and the reactive diluent utilized.

Table 1. Composition of the Photocurable Resins, the Corresponding Potential Biobased Content, Photoinitiator Amount, and the Respective Viscosity

resin name	PPH (wt %)	HEMA (wt %)	biobased content (%)	TPO amount/wt %[a]	viscosity (mPa·s)
PPH30	30.0	70.0	97.0	3.0	48.2 ± 0.08
PPH50	50.0	50.0	97.0	3.0	490.8 ± 0.9
PPH70	70.0	30.0	97.0	3.0	6270.5 ± 86.2

[a]The percentage of photoinitiator used was calculated based on the total mass of monomers in the resin (PPH + HEMA).

After MA melting, the temperature was increased up to 120 °C, and the reaction was carried out under stirring and an ambient atmosphere for 30 min, until a yellowish, homogeneous, and viscous product was formed (designated PP). The second synthesis used the same precursors, proportions, and temperatures. Nevertheless, after the temperature was raised to 120 °C, sulfuric acid (2 wt % relative to the total mass of GLY and MA) was added to the reaction vessel as a catalyst. The reaction time required to achieve the same previously visual characteristics was 8 min (determined to be the reaction end point). The resulting product, a colorless and highly viscous material, was designated PPH. Figure 1 exhibits the steps of this work and the structures proposed for prepolymers.

2.3. Formulation of the Photocurable Resins with Different Amounts of Prepolymer. All formulated resins were produced by mixing the PPH and the potential biobased acrylic monomer, HEMA, as a reactive diluent. For each composition, 100 g were prepared. Table 1 reports the composition of each resin, its name, and its biobased content (BC%), which was calculated using eq 1[28] where m_{PPH}, m_{HEMA}, and m_{TPO} are the masses in grams of each resin component. Due to its high viscosity, PPH was heated to 70 °C before adding HEMA. Both components were stirred to obtain a homogeneous mixture and then cooled to room temperature before printing and characterization. The type 1 photoinitiator TPO was added to all compositions (3 wt % of monomeric mixture weight) and the viscosity of all resins was measured. The scheme in Figure 1 illustrates the photopolymerization reaction product using the produced monomeric mixtures.

$$BC(\%) = \left[\frac{(m_{PPH} + m_{HEMA})}{(m_{PPH} + m_{HEMA} + m_{TPO})}\right] \times 100 \quad (1)$$

2.4. 3D Printing of the Resins. The 3D printing of the resins PPH30, PPH50, and PPH70 was performed in an Elegoo Mars 2 Pro DLP 3D printer equipped with a 405 nm light source (E_{max} = 3.8 mW cm^{-2}). After the printing, the pieces were detached, subsequently washed with isopropyl alcohol, and post-cured at room temperature for 30 min under ultraviolet (UV) irradiation (405 nm) using the equipment Elegoo Wash & Cure Mercury Plus. The 3D models were sliced, and the printing parameters, such as the exposure time and the layer thickness, were adjusted using Chitubox slicing software. Therefore, the settings applied (shown in Table 2) were kept the same for all systems exclusively to investigate the difference in the physical-chemical properties of the materials produced, since all resins were able to form solid materials within these conditions. The materials obtained from PPH30, PPH50, and PPH70 were called POL30, POL50, and POL70, respectively. Aiming to assess the printability of all resins, two objects with different designs (the Eiffel Tower and a dinosaur) and a height of 1.5 cm were produced. All characterizations were performed using fresh samples.

https://doi.org/10.1021/acssuschemeng.5c03006
ACS Sustainable Chem. Eng. 2025, 13, 9771−9782

Table 2. Printing Parameters to Produce the Designed Specimens from All Resins

printing parameters	settings
layer height	0.05 mm
base layer amount	18
exposure time for base layers	50 s
exposition time for the rest of the layers	15 s
elevation after printing	5 mm

2.5. Working Curves. The Jacobs working curves for the resins PPH30, PPH50, and PPH70 were acquired according to the literature.[29,30] One-layer squares with 10 mm of length and 10 mm of width were cured, varying the exposure time (15−100 s) in an Elegoo Mars 2 Pro DLP 3D printer in the absence of the printing platform and with a constant light intensity of 3.8 mW cm^{-2}. Each printed sample was washed with isopropyl alcohol to remove noncured resin, and its thickness was measured with a micrometer, resulting in the curing depth (C_d) for each exposure time. Jacobs working curves were generated as a semilogarithmic plot showing the dependence of cure depth on the exposure energy of the incident light on the resin surface (E_{max}). The Jacobs equation, based on the Lambert−Beer law (eq 2), offers a better understanding of the UV-curing process during printing by relating the penetration depth (D_p), determined by the slope of the curve, and the critical energy exposure dose (E_c) for the gel point, which is identified by the x-axis intercept.[30]

$$C_d = D_p \ln\left(\frac{E_{max}}{E_c}\right) \quad (2)$$

2.6. Characterization. *2.6.1. Viscosity Analysis.* The viscosity (η) of pure HEMA and the photocurable resins PPH30, PPH50, and PPH70 were analyzed in a digital rotary viscosimeter Brookfield DV-III rheometer (Brookfield, Toronto, Canada), with a water bath controlled at 27 °C. Due to the different viscosities observed in the samples, it was necessary to use different spindles (considering the specific interval of viscosity for each spindle). Then, the following spindles were used: SC4−18 for HEMA and PPH30 samples and SC4−34 for PPH50 and PPH70.

2.6.2. ^{1}H NMR Analysis. ^{1}H NMR spectra were obtained from an Agilent 400 MHz Premium Shield spectrometer. GLY, PP, and PPH were solubilized in deuterated water (D_2O, 99.9% D, Sigma-Aldrich).

2.6.3. Mid-Infrared Spectroscopy Analysis (MIR) and Monomer Conversion. MIR spectra were acquired using a Bruker Vertex 70 FT-IR spectrometer with an attenuated total reflectance diamond crystal accessory. The measurements were performed in the range of 4000−400 cm^{-1} with 32 scans and a 4 cm^{-1} resolution.

Monomer conversion to polymer (MC%) was evaluated using a previously described method.[31] All formulated resins, as well as 3D-printed (using the same parameters reported above) square bars with dimensions of 10 mm length, 10 mm width, and 2 mm thickness obtained from each resin, were submitted to this analysis. The total area of the C═C bond bands (present in PPH and HEMA) at 1635 cm^{-1} was measured before and after the printing process (and postcure process). The obtained spectra were normalized using the C−H methylene group stretching band at 2956 cm^{-1}. MC% values were then determined using eq 3.

$$MC\% = \left\{1 - \left[\frac{\left(\frac{A_{1635}}{A_{2956}}\right)_{t=x}}{\left(\frac{A_{1635}}{A_{2956}}\right)_{t=0}}\right] \times 100\right\} \quad (3)$$

A_{1635} is the total area of C═C band and A_{2956} corresponds to the total area of C−H band; $t = 0$ refers to the resin before the printing and $t = x$ to the material obtained after the printing (and postcure of 30 min).

2.6.4. Simultaneous Thermogravimetry−Differential Thermal Analysis (TG−DTA). Simultaneous TG−DTA curves were obtained

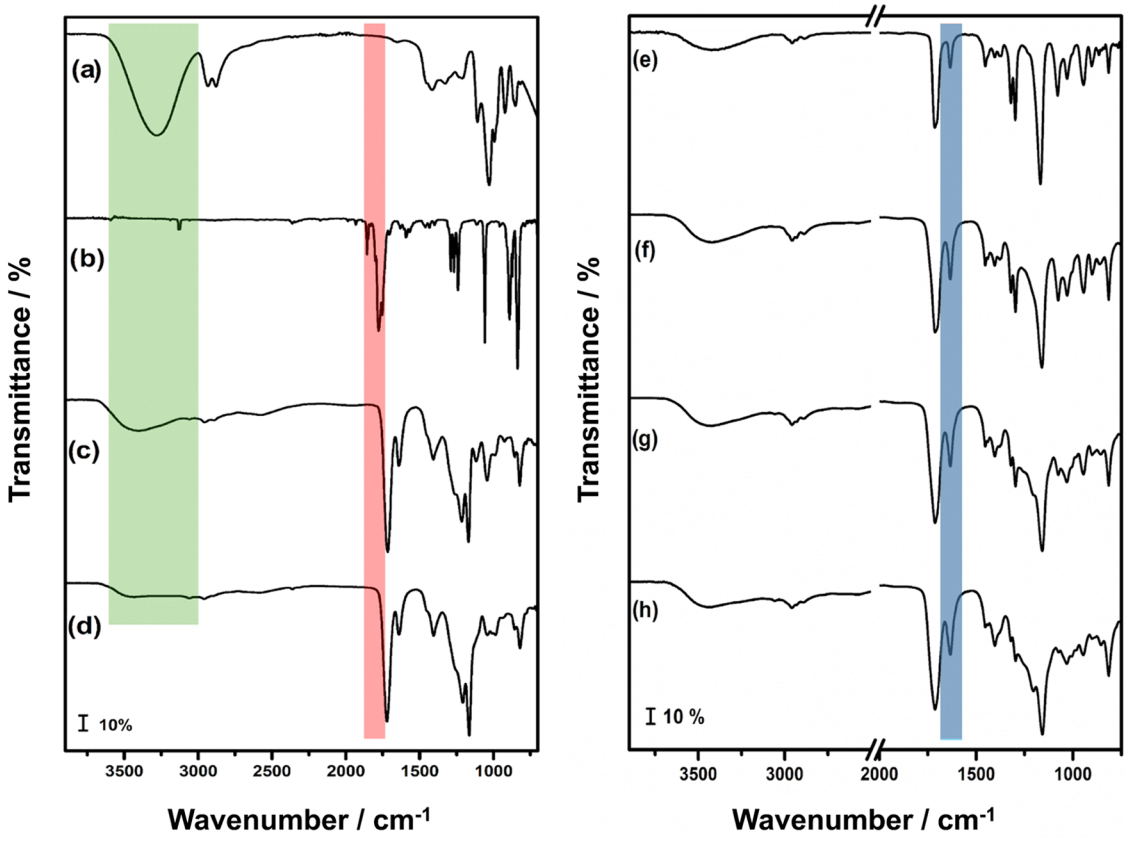

Figure 2. MIR spectra for (a) GLY, (b) MA, (c) PP, (d) PPH, (e) HEMA, and the formulated resins (f) PPH30, (g) PPH50, and (h) PPH70.

https://doi.org/10.1021/acssuschemeng.5c03006
ACS Sustainable Chem. Eng. 2025, 13, 9771−9782

in the STA 449 F3 equipment (Netzsch) using the following conditions: open α-alumina crucibles (200 μL), approximately 10 mg of sample (to each analyzed material), a temperature range of 30 to 800 °C, a dry air atmosphere (70 mL min^{-1}), and a heating rate of 10 °C min^{-1}.

2.6.5. Differential Scanning Calorimetry (DSC) and Photo-DSC. DSC analyses were performed on DSC1 Star^e equipment (Mettler-Toledo) using 5 mg of each sample, which was analyzed in a 40 μL closed aluminum crucible with a perforated lid and an air flow rate of 50 mL min^{-1}. Samples were heated from −10 to 100 °C with a heating rate of 10 °C min^{-1}. For photo-DSC, the same equipment was employed in isothermal mode (25 °C), air atmosphere, and a flow rate of 50 mL min^{-1}. Approximately 5 mg of each sample was cured in open aluminum crucibles with a Kessil KSPR160 (365 nm) at an intensity of 100% (E_{max} = 399 mW cm^{-2}). Two isothermal cycles of 2 min were performed for each sample, and the total energy involved in photopolymerization was determined after subtracting the first isothermal curve from the second.[29] The polymerization rate (R_p) was calculated based on eq 4, at the time of the exothermic polymerization peak, and considering the heat flow under an isothermal condition of 25 °C (dH/dt).[29]

$$R_p = \left(\frac{dH}{dt}\right)_T \quad (4)$$

2.6.6. Dynamic Mechanical Analysis (DMA). DMA analysis was performed in a Q800 apparatus (TA Instruments). Rectangular bars with dimensions of 20 mm length, 5 mm width, and 1 mm thickness were designed and 3D-printed. The analysis was performed from −30 to 100 °C at a heating rate of 3 °C min^{-1} and a frequency of 1 Hz. The DMA curves provided the storage modulus (E') and the tan δ values. The temperature at the peak of the α-transition in the tan δ curve was determined as the glass transition temperature.[32]

2.6.7. Gel Content. The gel content value (GC) for all 3D-printed materials was evaluated according to the procedure reported in the literature.[28] Each material was weighed, and the value was recorded as the initial weight (W_i). Subsequently, the respective material was added to a paper cartridge and then refluxed in a Soxhlet apparatus with acetone for 24 h. The resulting material was dried in an oven at 60 °C for 3 h, and the final weight (W_f) was recorded for determining the GC % according to eq 5.

$$GC(\%) = \left(\frac{W_f}{W_i}\right) \times 100 \quad (5)$$

2.6.8. Hardness. The hardness of the 3D-printed squares (60 mm length, 60 mm width, and 30 mm thickness) from each formulated resin was acquired using an analog Shore D durometer.

3. RESULTS AND DISCUSSION

3.1. MIR, ^{1}H NMR, Viscosity, Biobased Content, and Sustainable Metrics. The MIR spectra for GLY, MA, PP, and PPH are shown in Figure 2. After the reaction, the spectra of both PP and PPH presented a similar profile: a decrease in the band related to O−H stretching (green box) from glycerol, the total absence of asymmetric and symmetric C═O bands from anhydride (red box), and the appearance of new bands at 1720, 1635, and 1168 cm^{-1} corresponding to C═O, C═C, and C−O groups, respectively. The emergence of these bands suggests that a possible esterification reaction occurred, resulting in a product containing α,β-unsaturated esters. This is supported by the carbonyl group's absorption shift to a lower wavenumber than typically observed, resulting from the resonance effect.[33]

The MIR spectra for HEMA and the formulated resins PPH30, PPH50, and PPH70 are shown in Figure 2e,h. The resins exhibit similar spectral profiles; however, the intensity of the C═C stretching band at 1635 cm^{-1} is greater than in the corresponding precursors. This is expected due to the presence of these bonds in both HEMA and PPH. The spectra for the 3D-printed polymers POL30, POL50, and POL70 are provided in the Supporting Information (Figures S1−S3), and all materials retain a band at 1635 cm^{-1}, indicating incomplete photopolymerization. Consequently, the monomer conversion (MC %) was calculated for the polymers obtained after printing, with the results presented in Table 3. A decrease in MC% values is observed with increasing PPH content in the resin, aligning with the enthalpy variation verified by photo-DSC, further discussed in this work. It is hypothesized that the residual double bonds correspond to the alkenes in most PPH, located between two carbonyl groups, facilitating resonance and thus requiring longer photopolymerization times. Then, two monomer mixtures were prepared to test this hypothesis: one containing PPH with 3 wt % TPO, and another containing HEMA with 3 wt % TPO. These mixtures were photopolymerized for 15 s (replicating the 3D printing exposure time) under UV irradiation (365 nm, E_{max} = 399 mW cm^{-2}) at a distance of 1 mm. Subsequent MC% calculations revealed a value of 15.1% for PPH and a significantly higher value of 65.3% for HEMA. Thus, the polymerization of HEMA chains proceeds much more rapidly than that of PPH chains, as evidenced by this difference in reactivity.

Table 3. Physical-chemical Properties of all 3D-printed Polymers

	POL30	POL50	POL70
MC (%)	72	62	41
$T_{stability}$ (°C)	98.4	97.6	95.7
T_g (°C)	60.1	52.2	3.3
tan δ (°C)	61.0	50.2	9.7
GC (%)	71.0	59.2	43.3
maximum elongation (%)[a]	98.4	130.9	31.4
tensile strength (MPa)[a]	0.4	0.3	0.3
hardness (Shore D)	50.1	14.0	11.0

[a]Maximum elongation and tensile strength were determined at the point of maximum force, as the samples did not break under the experimental conditions performed.

Although the resins' MC% values differ significantly, all formulations were able to produce solid 3D-printed objects with different architectural complexities.

^{1}H NMR spectra for GLY, PP, and PPH are shown in Figure 3. The GLY spectrum (Figure 3a) exhibits a doublet of quartets between 3.46 and 3.59 ppm and a multiplet between 3.68 and 3.73 ppm. These signals correspond to the aliphatic hydrogens of the glycerol backbone. After reaction with MA, the spectra of both products show similar profiles, with signals between 3.81 and 4.24 ppm (highlighted in green), attributed to the glycerol backbone hydrogens now shifted due to the changed chemical environment, and between 6.17 and 6.47 ppm (highlighted in blue), corresponding to vinylic hydrogens. Besides, monosubstituted glycerol signals are verified between 3.51 and 3.54 ppm and at 3.69 ppm (dashed red boxes). Trisubstitution in PPH is attributed to the signals between 4.25 and 4.42 ppm, as well as at 5.15 ppm (dashed black boxes), which indicates that cross-linked structures were formed as illustrated in Figure S4. Furthermore, the absence of acid hydrogen signals in the 10.0−12.0 ppm region (Figure 3d) is noted.

Based on the proportional analysis of NMR signal integrations, the percentages of mono-, di-, and trisubstitution were determined for both products (Figures S5 and S6). The residual glycerol backbone quartet, observed between 3.44 and

https://doi.org/10.1021/acssuschemeng.5c03006
ACS Sustainable Chem. Eng. 2025, 13, 9771−9782

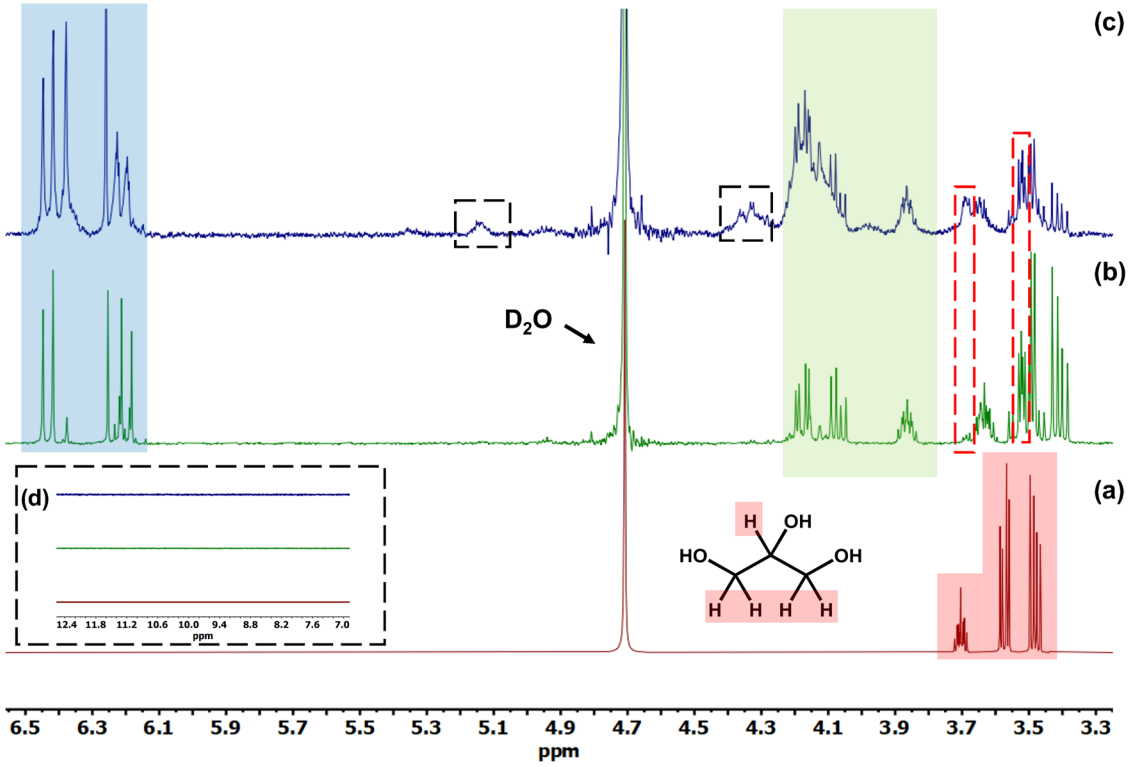

Figure 3. ^{1}H NMR spectra of (a) glycerol, (b) PP, and (c) PPH. Approximation of (d) acid protons region.

3.37 ppm, was integrated and standardized to 2.00 hydrogens. Subsequently, the signals corresponding to the three substitution states were integrated, accounting for chemical shift variations and subtracting overlapping signals.

For instance, in the case of PPH, the range between 3.46 and 3.54 ppm exhibited a total integration of 10.01, which includes contributions from both unmodified glycerol and monosubstituted glycerol hydrogens. After subtracting 2.00 (assigned to unmodified glycerol), 8.01 hydrogens remained, corresponding to the hydrogens on the carbon adjacent to the primary alcohol in the monosubstituted structure.

To determine the contribution from disubstituted glycerol, the integration value of 8.01 was subtracted from the total integration of the region between 3.81 and 4.24 ppm. This correction accounts for the overlap between mono- and disubstituted signals, particularly the hydrogens adjacent to the ester groups.

The relative proportions of each species were then calculated, yielding the following distribution for PPH: residual glycerol (4.5%), monosubstituted (18.1%), disubstituted (62.4%), and trisubstituted (15.0%). For PP, the same analytical procedure was applied, resulting in the following proportions: residual glycerol (42.2%), monosubstituted (37.6%), and disubstituted (20.2%).

According to residual glycerol content, the overall conversion for PPH and PP was determined to be 95.5 and 57.8%, respectively. Combined with the MIR results, it is suggested that esterification reaction occurred at both carbonyl carbons of MA, producing α,β-unsaturated dicarboxylic or tricarboxylic polyesters terminated with monosubstituted glycerol, as indicated in Figure S7 for PPH. The residual glycerol presence can be attributed to MA evaporation during the reaction.

These findings show that this approach was effective since, initially, the reaction time without a catalyst took around 30 min. During this time, sublimation of maleic anhydride was observed on the beaker walls. The addition of an acid catalyst reduced the reaction time to approximately 8 min, as well as MA evaporation issues, which allowed a higher conversion for PPH. It represents an important advance in using renewable resources to produce monomers since a similar compound obtained by Huang et al.[16] from the same precursors and without a catalyst took around 2 h at 140 °C to be formed.

Additionally, two sustainable metrics were determined for PPH:[34] reaction mass efficiency (RME) and *E*-factor. RME evaluates the efficiency of a chemical reaction by considering the mass of the obtained product and the reagents utilized.[35] The E-factor represents the environmental impact of a chemical process regarding waste generated, where a value of 0 (zero) indicates no impact or waste.[36] PPH exhibited an RME of 89.0% and an *E*-factor of 0.075, indicating a minimal waste generation[34] and consequently, a greener and more environmentally friendly profile.[37]

Due to the time advantage of PPH production and conversion, the formulation of all photocurable resins was conducted using this prepolymer.

Viscosity is a crucial parameter in 3D printing, directly affecting the resolution of printed objects and the amount of resin consumed (an economic consideration). As reported by Guggenbiller et al.[38] stereolithography (SLA) and digital light processing (DLP), resins typically require low viscosities, ranging from 0.1 to 10 Pa·s, and Newtonian fluid behavior. This allows the unreacted resin to flow out of negative spaces between layer illuminations and refill vacant spaces in the vat during printing. Figure S8 shows the shear stress dependence on the shear rate for HEMA, PPH30, PPH50, and PPH70. The observed linear behavior for all samples indicates Newtonian fluid behavior. Then, based on the linear regression of each curve, displayed in Figure S9, it was possible to find that the

https://doi.org/10.1021/acssuschemeng.5c03006
ACS Sustainable Chem. Eng. 2025, 13, 9771−9782

viscosity of HEMA is 5.4 ± 0.04 mPa·s. At the same time, the increase of PPH amount in the formulated resins led to a substantial viscosity increase, as presented in Table 1. This was expected, given the very high viscosity of PPH, which is attributed to strong intermolecular interactions, such as hydrogen bonds between the carbonyl groups and free hydroxyl groups from PPH[39] as presented in Figure 4. However, the addition of HEMA allows for new hydrogen interactions between PPH chains and this low molecular weight diluent, increasing the interstructural distance and consequently decreasing the viscosity.[40] Although pure HEMA, PPH, and PPH30 do not present a suitable viscosity for 3D printing, PPH50 and PPH70 resins exhibited viscosity values that fit with the recommendation for 3D printing. Moreover, as described below in this work, the low viscosity of PPH30 did not negatively impact the resolution of 3D-printed materials.

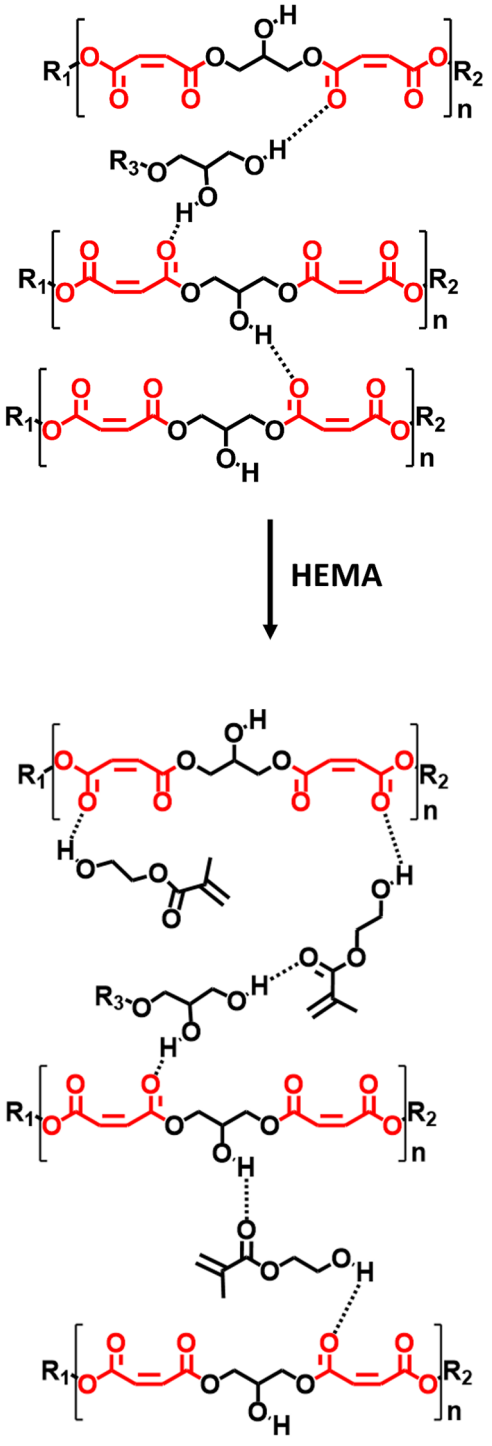

Figure 4. Scheme demonstrating the rearrangement of hydrogen bonds before and after HEMA addition.

Biobased monomers and polymers offer a significant pathway to reducing the environmental impact of fossil-based materials. Their production directly decreases the carbon footprint and contributes to carbon sequestration.[41] Biobased content (BC%), a parameter representing the percentage of biomass components in a product, quantifies this contribution, considering the product's total weight and the four main constituent atoms: carbon, hydrogen, oxygen, and nitrogen.[42] PPH has a 100% biobased content, as glycerol is a byproduct of biodiesel production (which uses vegetable oils as the primary raw material), and maleic anhydride can be produced from the oxidation of renewable furfural, which is derived from agricultural materials that do not compete with food or human consumption.[43] HEMA is also biobased, as its methacrylic and ethylene glycol components can be derived from natural sources.[22,23] However, TPO is not biobased and directly affects the BC% of the formulated resins, as shown in Table 1. Despite that, all resins presented a BC% value of 97%, greater than 20%, making them recognized as potentially biobased materials.[42]

Thus, considering the aspects of PPH and its respective derived resins it is suggested that these photocurable monomers (and monomeric mixtures) align with the following principles of Green Chemistry:[37] 1 (prevention), 5 (safer solvents and auxiliaries), 6 (design for energy efficiency), 7 (use of renewable feedstocks), and 9 (catalysis).

3.2. Photo-DSC, Working Curves, and 3D Printing.

Photo-DSC analysis was performed on all resins, PPH, and HEMA to assess the peak time (PT), heat release at the peak (ΔH_{HR}), total enthalpy (ΔH_T), and polymerization rate (R_p) of the photopolymerization reaction. As depicted in Figure 5a, HEMA exhibited a $\Delta_{HR} = 66.5$ J g^{-1}, an $R_p = 9.5$ s^{-1}, and a $\Delta H_T =$ 150.9 J g^{-1} after 120 s. In contrast, PPH showed the lowest enthalpy and polymerization rate values ($\Delta H_{HR} = 7.9$ J g^{-1}, $R_p =$ 0.6 s^{-1}, and $\Delta H_T = 62.5$ J g^{-1} after 120 s), indicating a lower degree of polymerization, consistent with MIR analysis. Nevertheless, a significant increase in these values was observed across all resins (Table 4), with PPH30 displaying the highest ΔH_{HR}, R_p, and ΔH_T values. This trend was attributed to the increased chain mobility of PPH, facilitating better diffusion in the propagation step during the polymerization and finally releasing more energy.[44]

The resin-intrinsic parameters E_c and D_p were investigated by Jacobs working curves as shown in Figure 5b and Table 4. Although critical energy exposure did not change significantly, the same trend verified previously is observed with PPH30, requiring the lowest E_c value to reach a gel point, indicating the highest reactivity. Moreover, these values are lower than those of other biobased acrylic resins reported in the literature.[45] Conversely, higher amounts of PPH in the resins led to higher D_p values, which can be attributed to slower polymerization as the active species have more time to diffuse deeper in the resin. These high D_p were associated with overcure as shown below.

Although working curves offer valuable information about printing conditions, a balance must be found between exposure time and interfacial adhesion in the building plate. Thus, after 3D-printing tests, it was verified that the conditions shown in

https://doi.org/10.1021/acssuschemeng.5c03006
ACS Sustainable Chem. Eng. 2025, 13, 9771−9782

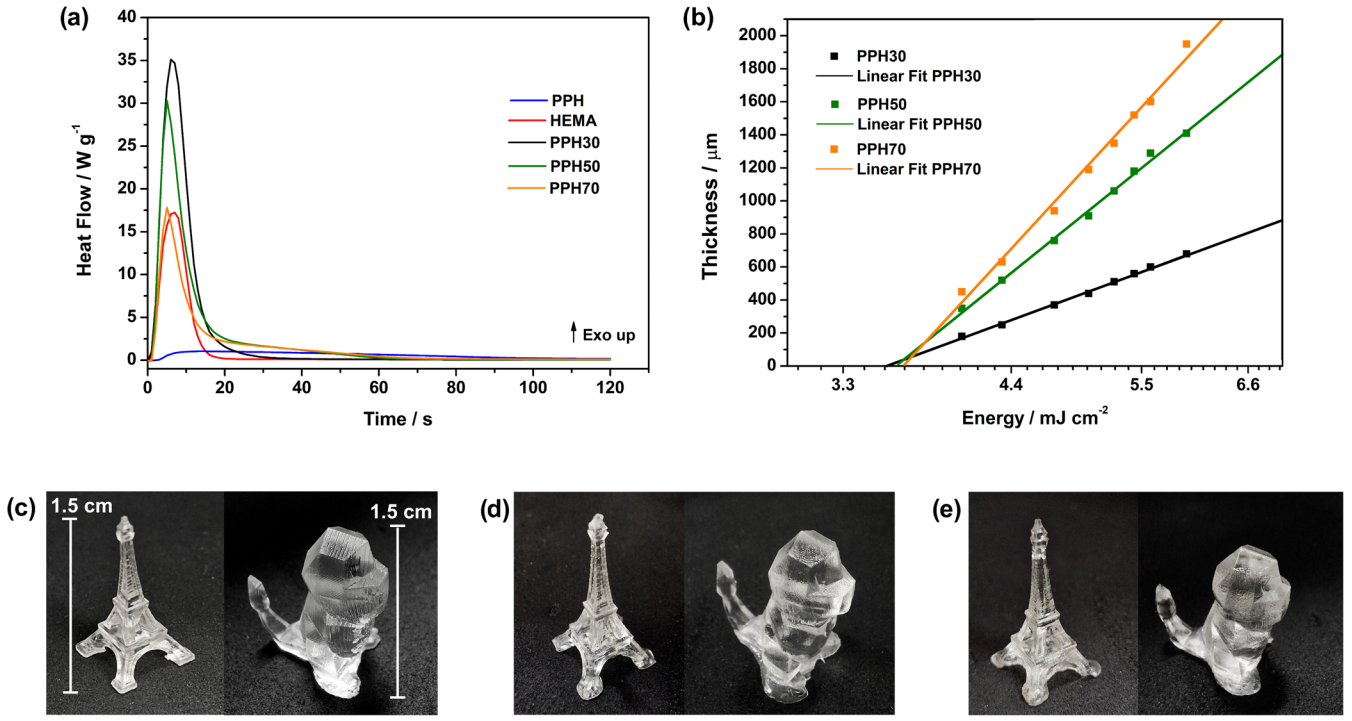

Figure 5. Investigation of monomer reactivity by (a) photo-DSC and (b) working curves for all resins. Eiffel Tower and dinosaur objects 3D-printed from (c) PPH30, (d) PPH50, and (e) PPH70 resins.

Table 4. Photo-DSC Results of All Formulated Resins, Including Heat Release at the Peak (ΔH_{HR}), Total Enthalpy (ΔH_T), Polymerization Rate (R_p), and Peak Time (PT)[a]

	photo-DSC				working curves		
resin	ΔH_{HR} (J g^{-1})	ΔH_T (J g^{-1})	R_p (s^{-1})	PT (s)	E_c (mJ cm^{-2})	D_p (μm)	R^2
PPH30	103.0	312.1	17.2	6.0	3.38	269.70	0.99
PPH50	60.6	283.9	12.1	5.0	3.43	578.94	0.99
PPH70	38.8	194.0	7.8	5.0	3.52	788.77	0.99

[a]Critical energy exposure dose (E_c), penetration depth (D_p), and coefficient of determination (R^2) obtained from working curves.

Table 2 were enough for a complete printing of objects. Figure 5c,f show the 3D-printed objects obtained from each formulated resin. The resolution seems to be affected by increasing PPH content in the formulation, depending on the complexity of the object. For example, the Eiffel Tower 3D-printed from PPH30 does not show any apparent qualitative defects. In contrast, a slight decrease in resolution is noticeable for the other formulated systems (PPH50 and PPH70) as the base of the tower is less defined. However, no difference was observed among the formulated resins for the dinosaur object. Furthermore, no cracks were observed in the material before and after the postcure process. Thus, all resins were able to form objects with different designs, making them suitable for use as potentially biobased resins for 3D printing.

A comb-shaped test structure (Figure 6a), incorporating cavities and squares with defined dimensions (as previously reported in the literature),[46] was designed to evaluate the resolution of 3D-printed objects produced from all resins, including a nonrenewable commercial resin (CR). Besides, as overcuring can directly affect the resolution of 3D-printed objects, this parameter was determined using eqs 6 and 7 adapted from Stevens et al.[47] In this work, it was suggested that overcure decreases the size of cavities and increases the lateral size of squares. Thus, the calculation considered the cavity radii and square widths using both theoretical values from the CAD model and empirical measurements from the 3D-printed object.

The resins were cured for 15 s per layer using the same equipment utilized in this work. Table S1 summarizes the radii and widths of the CAD model and those measured in the 3D-printed objects with a digital caliper.

$$\%\text{overcure}_{\text{cavity}} = \frac{\text{theoretical} - \text{actual}}{\text{theoretical}} \times 100 \quad (6)$$

$$\%\text{overcure}_{\text{square}} = \frac{\text{actual} - \text{theoretical}}{\text{theoretical}} \times 100 \quad (7)$$

As can be seen in Figure 6 and Table S1, all printed objects exhibited resolution in the millimeter range. However, increasing the PPH content in the resin negatively affected the resolution as the percentage of overcure increased, making it impossible to reach a required circular shape at the determined dimensions. In this case, it is suggested that high D_p and viscosity values are responsible for overcuring; nevertheless, as reported by Ballester-Bayarri et al.[48] an overcure optimization by adding a photo absorbent in the resins may reduce this effect.

Although CR exhibited improved resolution for cavity printing (Figure S10), it showed a higher %Overcure for square shapes compared to the renewable resins PPH30 and PPH50. A similar %Overcure for squares was observed in the PPH70 resin.

https://doi.org/10.1021/acssuschemeng.5c03006
ACS Sustainable Chem. Eng. 2025, 13, 9771−9782

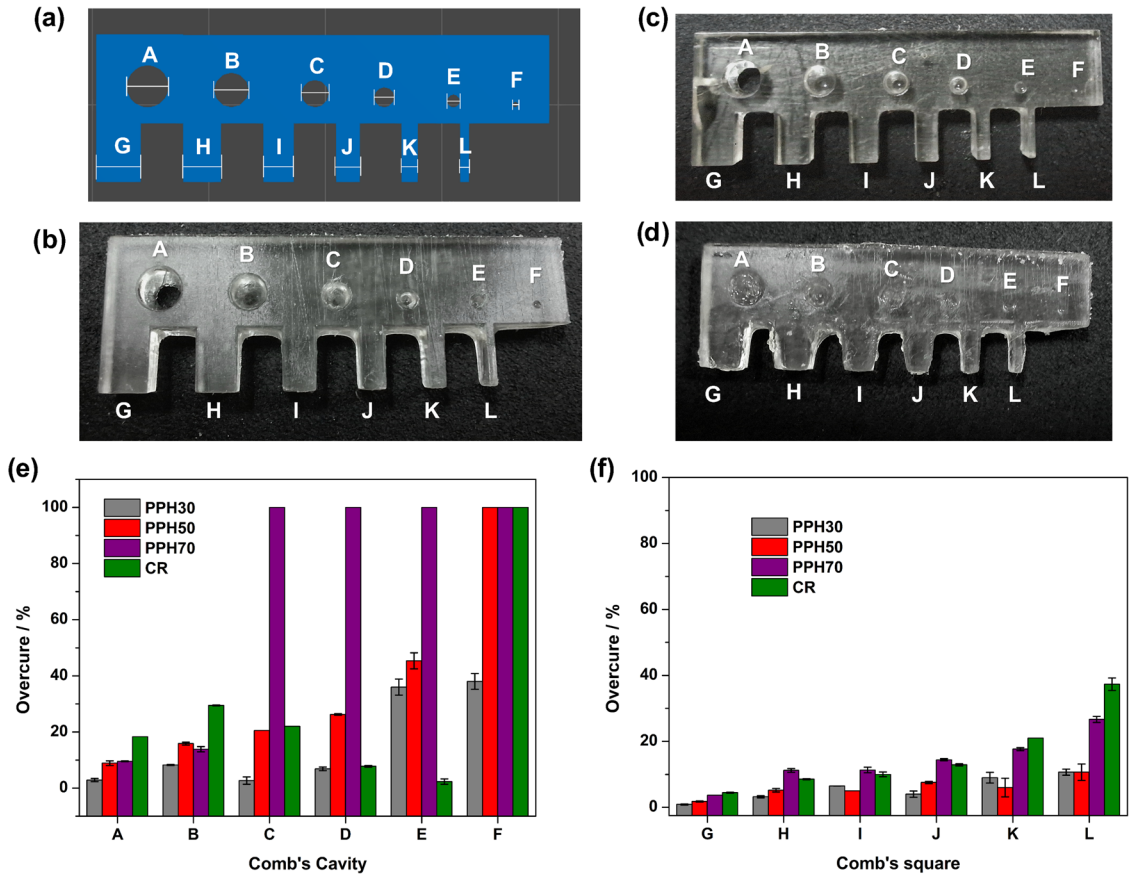

Figure 6. (a) CAD model of the comb-shaped test structure and 3D-printed objects using (b) PPH30, (c) PPH50, and (d) PPH70. Overcure percentage study for the resins developed and comparison with commercial resin (CR) regarding (e) the comb's cavity and (f) the comb's square.

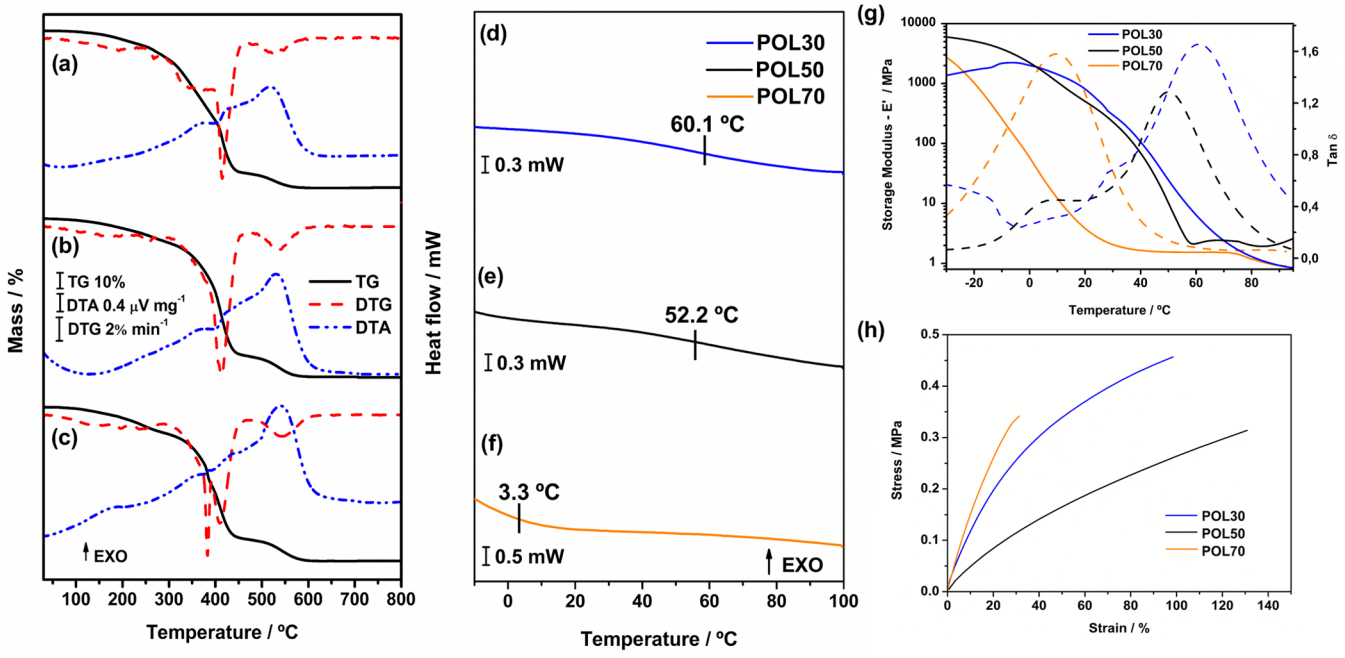

Figure 7. TG/DTG-DTA and DSC curves for (a, d) POL30, (b, e) POL50, and (c, f) POL70. (g) Relaxation and (h) stress−strain curves for the 3D-printed polymers.

Thus, all potentially biobased photocurable resins developed in this work are comparable to nonrenewable commercial resins, offering potential for 3D printing since overcure optimization is performed.

3.3. Gel Content and Thermal Analysis: TG/DTG-DTA, DSC, and DMA. According to eq 6, the gel content values (Table 3) for the polymeric materials obtained after printing exhibited a trend similar to that observed in the MC% values,

https://doi.org/10.1021/acssuschemeng.5c03006
ACS Sustainable Chem. Eng. 2025, 13, 9771−9782

with POL30 showing the highest value and POL70 the lowest. A possible explanation for this behavior is the lower reactivity of PPH, which results in fewer units of this prepolymer being cross-linked, while non-cross-linked or partially cross-linked units (monomers and oligomers) are leached out by the solvent.

The TG/DTG-DTA curves for 3D-printed materials using each formulated resin are displayed in Figure 7a−c, while the complete TG-DTA data is available in Table S2. The thermal profiles of all polymers are similar, exhibiting three mass loss steps. While the TG curve makes it difficult to discern the first and second steps, the DTG curves confirm their presence, with the second step exhibiting complex and overlapping events. The first mass loss step of all polymers can be attributed to a combination of evaporation and thermal degradation of PPH. This is supported by the TG/DTG-DTA curve of PPH (Figure S11a and Table S2) as well as its MIR spectra collected at different temperatures. In the first mass loss step, the prepolymer initially evaporates from 88.2 to 179.0 °C and undergoes degradation above this temperature since an endothermic and a subsequent exothermic event is observed in the DTA curve. These observations are supported by MIR analysis and visual changes verified in the pictures in Figure S11b. In this case, bubbles are verified in PPH after heating to 150 °C; however, no spectral changes are observed at this temperature, corroborating the evaporation process. Nevertheless, from 200 to 250 °C, the color of PPH began to change drastically, and the emergence of a new band at 1257 cm^{-1} and the disappearance of the band at 819 cm^{-1} were observed, suggesting structural changes caused by a degradation process.

The second mass loss step of the 3D-printed polymers corresponds to the degradation of the cross-linked polymeric matrix. The DTA curves show at least two exothermic peaks for this step. Finally, the third step, also accompanied by an exothermic event in the DTA curve, can be related to the decomposition of carbonaceous material by O_2. Table 3 shows that thermal stability ($T_{stability}$) decreases with increasing PPH in the formulated resins. This trend also aligns with the observed decrease in MC% values, which facilitates PPH evaporation/degradation.

DSC analyses shown in Figure 7 present the events observed during the heating stage (0−100 °C) of the 3D-printed polymers. The glass transition temperature (T_g) is shown to be above 50.0 °C for POL30 and POL50, while the lowest value is observed for POL70, as indicated by the midpoint in Figure 7d−f. These substantial differences between POL70 and the other polymers can be attributed primarily to the difference in MC% and second to the PPH characteristics. Furthermore, except for POL30, all materials are flexible at room temperature, indicating that a possible second-order transition can occur at lower temperatures, as confirmed by DMA analyses (described below). This may explain why the transitions observed in the DSC curves are extended since they start at temperatures lower than 20 °C, promoting overlapping events.

According to relaxation curves (Figure 7g), the temperature at the peak of the α-transition in the tan δ curve is higher for POL30, while POL70 presents the lowest value. These findings agree with the T_g values found in DSC curves. The transitions occurring at high temperatures can result from an entanglement in the polymeric network, formed by cross-linked HEMA and PPH, since polymers from pure HEMA present T_g values above 80 °C.[49,50] Additionally, second-order transitions are observed in POL30 and POL50 at 28.1 and 4.2 °C, respectively. These secondary transitions appear to be influenced by rigidity and MC% values, as POL30 exhibited a higher temperature value than POL50. Furthermore, the amount of PPH affects the intensity of tan δ, which is higher in POL50 than in POL30. This difference in tan δ intensity is attributed to the different amount of PPH in the resins. Thus, considering that PPH's reactivity is lower than HEMA and the presence of secondary transitions, which are influenced by the amount of each monomer, it is suggested that the materials generated can be primarily a traditional semi-interpenetrating polymer network.[51,52]

The unusual modulus behavior observed primarily for POL50 after the tan δ peak was investigated by subjecting the polymer to a heating process similar to that from DMA analysis. POL50 was heated from −30 to 100 °C at 3 °C min^{-1}, and MIR spectra were recorded before and after this process (Figure S12). Considering the normalized spectra, a decrease in the C═C band was noticed with an MC value of 35%. Thus, it is suggested that the observed modulus behavior likely resulted from residual polymerization induced by the heating process.

Stress−strain curves obtained at 25.0 °C are displayed in Figure 7h. It was observed that the maximum elongation of the polymer decreases with a high PPH content (equal to or above 70.0%) in the 3D-printed sample, while the tensile strength is maintained. This can be explained by PPH's low conversion and cross-linked points formation, respectively. Simultaneously, the strain is favored when 50.0% PPH is used, achieving a deformation of 130.0%.

Table 3 shows a decrease in hardness with increasing PPH content in the material. While this parameter seems to be influenced primarily by MC% values, it is suggested that the size of PPH chains can also contribute to the decrease in hardness, as the prepolymer units are longer than the monomer HEMA, decreasing the network packing and leading to softer materials.

4. CONCLUSIONS

A 100% renewable monomer was successfully synthesized from glycerol and maleic anhydride via a solvent-free and one-pot reaction. The reaction time was optimized to 8 min, and the conversion was increased to 95.5% with the addition of sulfuric acid as an esterification catalyst. The monomer's structure was elucidated, revealing that each unit of the product is an α,β-unsaturated dicarboxylic or tricarboxylic polyester terminated with monosubstituted glycerol. Due to these features, this renewable monomer was used in the formulation of high biobased content photocurable resins for 3D printing employing HEMA as a reactive diluent and then overcoming viscosity issues related to the very viscous product obtained. Increasing the PPH content in the resin formulation, the resolution of complex 3D-printed objects was slightly negatively affected, while robust materials with high biobased content could be produced with accuracy. This novel approach to potentially biobased photocurable resins enabled the production of renewable 3D printed materials with high biobased content.

The gel content, thermal, and mechanical properties of the 3D-printed material from each formulated resin are affected by monomer conversion as well as the amount of PPH in the formulation. Due to the difference in the reactivity of PPH and HEMA, it is suggested that the resulting material can be primarily a traditional semi-interpenetrating polymer network.

Overall, all resins formulated exhibited printability features due to the fast-curing process verified by photo-DSC and working curves, as well as suitability for greener additive manufacturing. This research represents an advance in the synthesis and application of a renewable acrylic polyester

https://doi.org/10.1021/acssuschemeng.5c03006
ACS Sustainable Chem. Eng. 2025, 13, 9771−9782

monomer derived from renewable resources for the sustainable production of materials, aligning with the principles 5, 6, 7, and 9 of Green Chemistry. Furthermore, the present approach opens a new window for future studies focused on property optimization and the application of these polymeric materials as covalent adaptable networks (CANs).

■ ASSOCIATED CONTENT

Supporting Information

The Supporting Information is available free of charge at https://pubs.acs.org/doi/10.1021/acssuschemeng.5c03006.

MIR spectra; ^{1}H NMR spectra; viscosity curves (shear stress vs shear rate); linear regression from viscosity measurements; information about the TG-DTA analyses; a comb-shaped test structure 3D-printed using a commercial resin; and a table containing the measurements of the comb-shaped test structures (PDF)

■ AUTHOR INFORMATION

Corresponding Author

Gilbert Bannach − *Universidade Estadual Paulista (UNESP), Faculdade de Ciências, Bauru 17033-260 SP, Brazil;* orcid.org/0000-0002-8790-5069; Email: gilbert.bannach@unesp.br

Authors

Gabriel I. dos Santos − *Universidade Estadual Paulista (UNESP), Faculdade de Ciências, Bauru 17033-260 SP, Brazil;* orcid.org/0000-0002-0307-203X

Caroline Gaglieri − *Universidade Estadual Paulista (UNESP), Faculdade de Ciências, Bauru 17033-260 SP, Brazil;* orcid.org/0000-0001-9612-6887

Rafael T. Alarcon − *Universidade de São Paulo (USP), Instituto de Química de São Carlos, São Carlos 13566-590 SP, Brazil;* orcid.org/0000-0003-2798-9587

Aniele de Moura − *Universidade de São Paulo (USP), Instituto de Química de São Carlos, São Carlos 13566-590 SP, Brazil;* orcid.org/0000-0002-3475-6207

Fernanda B. dos Santos − *Universidade Estadual Paulista (UNESP), Faculdade de Ciências, Bauru 17033-260 SP, Brazil;* orcid.org/0009-0006-1990-1492

Complete contact information is available at: https://pubs.acs.org/10.1021/acssuschemeng.5c03006

Author Contributions

The manuscript was written through the contributions of all authors. All authors have approved the final version of the manuscript.

Funding

The Article Processing Charge for the publication of this research was funded by the Coordenacao de Aperfeicoamento de Pessoal de Nivel Superior (CAPES), Brazil (ROR identifier: 00x0ma614).

Notes

The authors declare no competing financial interest.

■ ACKNOWLEDGMENTS

The authors wish to thank the São Paulo Research Foundation—FAPESP (grants 2024/14279-1; 2024/00779-2; 2024/03936-1; 2023/14645-5; 2021/14879-0) and the National Council for Scientific and Technological Development—CNPq (grant 303968/2024-9) for financial support.

■ REFERENCES

(1) Jadaun, J. S.; Bansal, S.; Sonthalia, A.; Rai, A. K.; Singh, S. P. Biodegradation of Plastics for Sustainable Environment. *Bioresour. Technol.* **2022**, *347*, No. 126697.

(2) Singh, N.; Ogunseitan, O. A.; Wong, M. H.; Tang, Y. Sustainable Materials Alternative to Petrochemical Plastics Pollution: A Review Analysis. *Sustainable Horiz.* **2022**, *2*, No. 100016.

(3) Pellis, A.; Malinconico, M.; Guarneri, A.; Gardossi, L. Renewable Polymers and Plastics: Performance beyond the Green. *New Biotechnol.* **2021**, *60*, 146−158.

(4) Maulana, S.; Wibowo, E. S.; Mardawati, E.; Iswanto, A. H.; Papadopoulos, A.; Lubis, M. A. R. Eco-Friendly and High-Performance Bio-Polyurethane Adhesives from Vegetable Oils: A Review. *Polymers* **2024**, *16* (11), No. 1613.

(5) Zhang, H.; Wu, J.; Guo, J.; Hu, J. Natural Terpenoid-Based Sustainable Thermoplastics, Cross-Linked Polymers, and Supramolecular Materials. *Polym. Rev.* **2024**, *64* (1), 119−161.

(6) Forrester, M.; Becker, A.; Hohmann, A.; Hernandez, N.; Lin, F.-Y.; Bloome, N.; Johnson, G.; Dietrich, H.; Marcinko, J.; Williams, R. C.; Cochran, E. RAFT Thermoplastics from Glycerol: A Biopolymer for Development of Sustainable Wood Adhesives. *Green Chem.* **2020**, *22* (18), 6148−6156.

(7) Ben, Z. Y.; Samsudin, H.; Yhaya, M. F. Glycerol: Its Properties, Polymer Synthesis, and Applications in Starch Based Films. *Eur. Polym. J.* **2022**, *175*, No. 111377.

(8) Kholif, A. E. Glycerol Use in Dairy Diets: A Systemic Review. *Anim. Nutr.* **2019**, *5* (3), 209−216.

(9) Wang, H.; Li, H.; Lee, C. K.; Nanyan, N. S. M.; Tay, G. S. A Systematic Review on Utilization of Biodiesel-Derived Crude Glycerol in Sustainable Polymers Preparation. *Int. J. Biol. Macromol.* **2024**, *261*, No. 129536.

(10) Cucciniello, R.; Cespi, D.; Riccardi, M.; Neri, E.; Passarini, F.; Pulselli, F. M. Maleic Anhydride from Bio-Based 1-Butanol and Furfural: A Life Cycle Assessment at the Pilot Scale. *Green Chem.* **2023**, *25* (15), 5922−5935.

(11) Müller, M.; Kutscherauer, M.; Böcklein, S.; Wehinger, G. D.; Turek, T.; Mestl, G. Modeling the Selective Oxidation of N-Butane to Maleic Anhydride: From Active Site to Industrial Reactor. *Catal. Today* **2022**, *387*, 82−106.

(12) Agirre, I.; Gandarias, I.; Granados, M. L.; Arias, P. L. Process Design and Techno-Economic Analysis of Gas and Aqueous Phase Maleic Anhydride Production from Biomass-Derived Furfural. *Biomass Convers. Biorefin.* **2020**, *10* (4), 1021−1033.

(13) Kolbuk, D.; Jeznach, O.; Wrzecionek, M.; Gadomska-Gajadhur, A. Poly(Glycerol Succinate) as an Eco-Friendly Component of PLLA and PLCL Fibres towards Medical Applications. *Polymers* **2020**, *12* (8), No. 1731.

(14) Magri, R.; Gaglieri, C.; Alarcon, R. T.; dos Santos, G. I.; Bannach, G. From Patauá Oil to Sustainable Polymers: Investigation of Epoxy/Anhydride Crosslink in Different Proportions. *J. Polym. Environ.* **2023**, *32* (3), 1453−1468.

(15) Magri, R.; Gaglieri, C.; Alarcon, R. T.; dos Santos, G. I.; Bannach, G. Eco-Friendly Polymers Based on Baru Vegetable Oil and Fumaric Acid Using Photopolymerization. *J. Polym. Res.* **2023**, *30* (6), No. 236.

(16) Huang, Y.; Jin, T.; Zeng, H.; Liu, L.; Xu, K.; Chai, X.; Xie, L.; Lin, Y.; Du, G.; Zhang, L. Development of Novel Sustainable Hyperbranched Polyester Wood Adhesives from Glycerol and Maleic Anhydride by Solvent Free Method. *Ind. Crops Prod.* **2023**, *204*, No. 117326.

(17) Martha, R.; Mubarok, M.; Batubara, I.; Rahayu, I. S.; Setiono, L.; Darmawan, W.; Akong, F. O.; George, B.; Gérardin, C.; Gérardin, P. Effect of Glycerol-Maleic Anhydride Treatment on Technological Properties of Short Rotation Teak Wood. *Wood Sci. Technol.* **2021**, *55* (6), 1795−1819.

(18) Yahyaee, S. M. H.; Dastoorian, F.; Ghorbani, M.; Zabihzadeh, S. M. Combined Effect of Organosolv Delignification/Polymerization on the Set Recovery of Densified Poplar Wood. *Eur. J. Wood Wood Prod* **2022**, *80*, 367−375.

(19) Alarcon, R. T.; dos Santos, G. I.; Gaglieri, C.; de Moura, A.; Cavalheiro, É. T. G.; Bannach, G. Lipidic Biomass as a Renewable Chemical Building Block for Polymeric Materials. *Chem. Commun.* **2024**, *60* (98), 14557−14572.
(20) Buratti, V. V.; Sanz, A.; Maturi, M.; Sambri, L.; Molina, S. I.; Franchini, M. C. Itaconic-Acid-Based Sustainable Poly(Ester Amide) Resin for Stereolithography. *Macromolecules* **2022**, *55* (8), 3087−3095.
(21) Maturi, M.; Spanu, C.; Locatelli, E.; Sambri, L.; Franchini, M. C. Myrcene-Itaconate Diels-Alder Cycloadducts in the Synthesis of Photocurable Polyesters for the 3D Printing of Fully Biobased Resins. *Addit. Manuf.* **2024**, *92*, No. 104360.
(22) Wang, Y.; Xian, M.; Feng, X.; Liu, M.; Zhao, G. Biosynthesis of Ethylene Glycol from D-Xylose in Recombinant *Escherichia Coli*. *Bioengineered* **2018**, *9* (1), 233−241.
(23) Le Nôtre, J.; Dijk, S. C. M. W.; van Haveren, J.; Scott, E. L.; Sanders, J. P. M. Synthesis of Bio-Based Methacrylic Acid by Decarboxylation of Itaconic Acid and Citric Acid Catalyzed by Solid Transition-Metal Catalysts. *ChemSusChem* **2014**, *7* (9), 2712−2720.
(24) Ng, T. S.; Norman, A.; Mohd, H.; Chong, C. H.; Cheah, K. H.; Yap, T. C.; Wong, V.-L. 3D Printing and Optimization of Biocompatible and Hydrophilic PEGDA-HEMA Lattice for Enhanced RhB Dye Removal from Aqueous Solution. *Int. J. Polym. Sci.* **2024**, *2024* (1), No. 6633503.
(25) Cui, J.; Liu, F.; Lu, Z.; Feng, S.; Liang, C.; Sun, Y.; Cui, J.; Zhang, B. Repeatedly Recyclable 3D Printing Catalyst-Free Dynamic Thermosetting Photopolymers. *Adv. Mater.* **2023**, *35* (20), No. 2211417.
(26) Resina 3D Azul. 3D Fila. https://3dfila.com.br/produto/resina-3d-azul-opaca/. (accessed January 10, 2025).
(27) Pires, O. A. B.; Alarcon, R. T.; Gaglieri, C.; da Silva-Filho, L. C.; Bannach, G. Synthesis and Characterization of a Biopolymer of Glycerol and Macadamia Oil. *J. Therm. Anal. Calorim.* **2019**, *137* (1), 161−170.
(28) Alarcon, R. T.; Gaglieri, C.; Bannach, G.; Cavalheiro, É. T. G. Greener Preparation of a Flexible Material Based on Macaw Palm Oil Derivatives and CO2. *Green Chem.* **2024**, *26* (6), 3261−3270.
(29) Alarcon, R. T.; Bergoglio, M.; Gomes, T.; Sangermano, M. Thiol-Ene Photopolymerization and 3D Printing of Non-Modified Castor Oil Containing Bio-Based Cellulosic Fillers. *Polymers* **2025**, *17* (5), No. 587.
(30) Shaukat, U.; Thalhamer, A.; Rossegger, E.; Schlögl, S. Dual-Vat Photopolymerization 3D Printing of Vitrimers. *Addit. Manuf.* **2024**, *79*, No. 103930.
(31) dos Santos, G. I.; Gaglieri, C.; Alarcon, R. T.; Magri, R.; Hartlieb, M.; Bannach, G. Passion Fruit Seed Oil: A Sustainable Feedstock for Additive Manufacturing of Renewable Polymers. *J. Polym. Environ.* **2024**, *32* (9), 4748−4762.
(32) Dong, J.; Liu, B.; Ding, H.; Shi, J.; Liu, N.; Dai, B.; Kim, I. Bio-Based Healable Non-Isocyanate Polyurethanes Driven by the Cooperation of Disulfide and Hydrogen Bonds. *Polym. Chem.* **2020**, *11* (47), 7524−7532.
(33) Pavia, D. L.; Lampman, G. M.; Kriz, G. S.; Vyvyan, J. R. *Introduction to Spectroscopy*, 5th ed.; Cengage Learning Asia Pte. Ltd: Taipei, 2015; p 54.
(34) Sahoo, S.; Dinda, T. K.; Mal, P. Dynamic Self-Assembled Systems of Photoinert *N*-Propargyl Amides Enable Red-Light Supramolecular Photocatalysis. *ACS Appl. Polym. Mater.* **2025**, *13*, 6258−6266.
(35) Sheldon, R. A. Metrics of Green Chemistry and Sustainability: Past, Present, and Future. *ACS Sustainable Chem. Eng.* **2018**, *6* (1), 32−48.
(36) Sheldon, R. A.; Bode, M. L.; Akakios, S. G. Metrics of Green Chemistry: Waste Minimization. *Curr. Opin. Green Sustainable Chem.* **2022**, *33*, No. 100569.
(37) Anastas, P.; Eghbali, N. Green Chemistry: Principles and Practice. *Chem. Soc. Rev.* **2010**, *39* (1), 301−312.
(38) Guggenbiller, G.; Brooks, S.; King, O.; Constant, E.; Merckle, D.; Weems, A. C. 3D Printing of Green and Renewable Polymeric Materials: Toward Greener Additive Manufacturing. *ACS Appl. Polym. Mater.* **2023**, *5* (5), 3201−3229.
(39) Lemon, M. T.; Jones, M. S.; Stansbury, J. W. Hydrogen Bonding Interactions in Methacrylate Monomers and Polymers. *J. Biomed. Mater. Res., Part A* **2007**, *83A* (3), 734−746.
(40) Li, J.; Cui, Y.; Qin, K.; Yu, J.; Guo, C.; Yang, J.; Zhang, C.; Jiang, D.; Wang, X. Synthesis and Properties of a Low-Viscosity UV-Curable Oligomer for Three-Dimensional Printing. *Polym. Bull.* **2016**, *73* (2), 571−585.
(41) Terry, J. S.; Taylor, A. C. The Properties and Suitability of Commercial Bio-Based Epoxies for Use in Fiber-Reinforced Composites. *J. Appl. Polym. Sci.* **2021**, *138* (20), No. 50417.
(42) ISO 16620−5. *Plastics—Biobased Content—Part 5: Declaration of Biobased Carbon Content, Biobased Synthetic Polymer Content and Biobased Mass Content* British Standards Institution: London; 2017.
(43) Lan, J.; Chen, Z.; Lin, J.; Yin, G. Catalytic Aerobic Oxidation of Renewable Furfural to Maleic Anhydride and Furanone Derivatives with Their Mechanistic Studies. *Green Chem.* **2014**, *16* (9), 4351−4358.
(44) Young, J. S.; Kannurpatti, A. R.; Bowman, C. N. Effect of Comonomer Concentration and Functionality on Photopolymerization Rates, Mechanical Properties and Heterogeneity of the Polymer. *Macromol. Chem. Phys.* **1998**, *199* (6), 1043−1049.
(45) Vazquez-Martel, C.; Becker, L.; Fiedler, B.; Elsner, P.; Blasco, E. Vegetable Oils as Sustainable Inks for Additive Manufacturing: A Comparative Study. *ACS Sustainable Chem. Eng.* **2021**, *9* (49), 16840−16848.
(46) Cazin, I.; Ocepek, M.; Kecelj, J.; Stražar, A. S.; Schlögl, S. Synthesis of Bio-Based Polyester Resins for Vat Photopolymerization 3D Printing. *Materials* **2024**, *17* (8), No. 1890.
(47) Stevens, L. M.; Recker, E. A.; Zhou, K. A.; Garcia, V. G.; Mason, K. S.; Tagnon, C.; Abdelaziz, N.; Page, Z. A. Counting All Photons: Efficient Optimization of Visible Light 3D Printing. *Adv. Mater. Technol.* **2023**, *8* (23), No. 2300052.
(48) Ballester-Bayarri, L.; Pascal, A.; Ayestaran, J.; Gonzalez, A.; Ballard, N.; Aguirresarobe, R. 3D Printing of Vinylogous Urethane-Based Methacrylic Covalent Adaptable Networks by Vat Photopolymerization. *ACS Appl. Polym. Mater.* **2024**, *6* (5), 2594−2603.
(49) Çaykara, T.; Özyürek, C.; Kantoğlu, Ö.; Erdoğan, B. Thermal Behavior of Poly(2-Hydroxyethyl Methacrylate-Maleic Acid) Networks. *Polym. Degrad. Stab.* **2003**, *80* (2), 339−343.
(50) Karabanova, L. V.; Sergeeva, L. M.; Svyatyna, A. V.; Yakushev, P. N.; Egorova, L. M.; Ryzhov, V. A.; Bershtein, V. A. Heterogeneity of Glass Transition Dynamics in Polyurethane-Poly(2-Hydroxyethyl Methacrylate) Semi-Interpenetrating Polymer Networks. *J. Polym. Sci., Part B:Polym. Phys.* **2007**, *45* (8), 963−975.
(51) Wang, M.; Jiang, J.; Liang, S.; Sui, C.; Wu, S. Functional Semi-Interpenetrating Polymer Networks. *Macromol. Rapid Commun.* **2024**, *45* (24), No. 2400539.
(52) Bartolotta, A.; Di Marco, G.; Lanza, M.; Carini, G.; D'Angelo, G.; Tripodo, G.; Fainleib, A.; Danilenko, I.; Grytsenko, V.; Sergeeva, L. Thermal and Mechanical Properties of Simultaneous and Sequential Full-Interpenetrating Polymer Networks. *Mater. Sci. Eng., A* **2004**, *370* (1−2), 288−292.

https://doi.org/10.1021/acssuschemeng.5c03006
ACS Sustainable Chem. Eng. 2025, 13, 9771−9782